Virology 476 (2015) 206–216

Contents lists available at ScienceDirect

Virology

journal homepage: www.elsevier.com/locate/yviro

Replication-competent influenza A viruses expressing a red fluorescent protein

Aitor Nogales [1], Steven F. Baker [1], Luis Martínez-Sobrido *

Department of Microbiology and Immunology, University of Rochester, Rochester, NY, United States

ARTICLE INFO

Article history:
Received 24 October 2014
Returned to author for revisions
25 November 2014
Accepted 2 December 2014
Available online 30 December 2014

Keywords:
Influenza A virus
NS1
mCherry
Replication-competent virus
2A
Neutralizing antibodies
Microneutralization assay
Virus neutralization assay
Antivirals
Interferon
In vivo imaging system (IVIS)

ABSTRACT

Like most animal viruses, studying influenza A in model systems requires secondary methodologies to identify infected cells. To circumvent this requirement, we describe the generation of replication-competent influenza A red fluorescent viruses. These influenza A viruses encode mCherry fused to the viral non-structural 1 (NS1) protein and display comparable growth kinetics to wild-type viruses *in vitro*. Infection of cells with influenza A mCherry viruses was neutralized with monoclonal antibodies and inhibited with antivirals to levels similar to wild-type virus. Influenza A mCherry viruses were also able to lethally infect mice, and strikingly, dose- and time-dependent kinetics of viral replication were monitored in whole excised mouse lungs using an *in vivo* imaging system (IVIS). By eliminating the need for secondary labeling of infected cells, influenza A mCherry viruses provide an ideal tool in the ongoing struggle to better characterize the virus and identify new therapeutics against influenza A viral infections.

Introduction

Influenza A virus (IAV), a member of the family *Orthomyxoviridae*, is a human respiratory pathogen that causes annual epidemics and occasional pandemics of considerable public health and economic impact (Molinari et al., 2007). The 20th century was marred by three documented influenza A pandemics: the Spanish flu (H1N1) of 1918, the Asian flu (H2N2) of 1957 and the Hong Kong flu (H3N2) of 1968, which together resulted in upwards of 60 million deaths (Kilbourne, 2006). The first influenza pandemic of the 21st century was declared in 2009 after the emergence of a quadruple-reassortant swine-origin H1N1 IAV that in less than one year infected more than 600,000 people worldwide (Louie et al., 2011; Smith et al., 2009). Additionally, the emergence of avian IAV strains that infect humans sporadically, such as H5N1, H7N9, and H10N8 have heightened worldwide concerns for pandemic preparedness, and together with the 2009 pandemic H1N1 IAV, provide credence for the improvement in monitoring, preventing and treating IAV infections (Ali et al., 2000; Herfst et al., 2012; Lopez-Martinez et al., 2013; Uyeki and Cox, 2013).

The IAV genome contains eight single-stranded RNA molecules of negative polarity, which are encapsidated into distinct viral ribonucleoprotein (vRNP) particles that contain the viral polymerase subunits PB2, PB1 and PA and multiple copies of the viral nucleoprotein (NP) (Palese, 2007). Genome replication and transcription occurs in the nucleus of infected cells and requires the tripartite polymerase complex, NP, and viral RNA (vRNA) (Wright et al., 2007). Reverse genetics, or the ability to rescue recombinant viruses from plasmid DNA, requires vRNA expression of all eight genome segments and protein expression of the aforementioned PB2, PB1, PA and NP (Fodor et al., 1999; Neumann et al., 1999). This approach has provided an excellent tool to study IAV biology (Ozawa and Kawaoka, 2011) and to develop a new generation of IAV vaccines (Martinez-Sobrido and Garcia-Sastre, 2010). Furthermore, modification of the IAV genome has resulted in replication-incompetent (Baker et al., 2013; Martinez-Sobrido et al., 2010) or -competent viruses that express foreign genes, including several reporter genes, which are expressed as fusion products to viral proteins (Avilov et al., 2012; Heaton et al., 2013; Kittel et al., 2004; Lakdawala et al., 2014; Li et al., 2010; Manicassamy et al., 2010; Martinez-Sobrido et al., 2010; Ozawa et al., 2011; Pan et al., 2013; Pena et al., 2013; Rimmelzwaan et al., 2007; Tran et al., 2013). An IAV protein commonly targeted for such genetic manipulation is

* Correspondence to: Department of Microbiology and Immunology, University of Rochester, School of Medicine and Dentistry, 601 Elmwood Avenue, Rochester, NY 14642, United States. Tel.: +1 585 276 4733.
E-mail address: luis_martinez@urmc.rochester.edu (L. Martínez-Sobrido).
[1] These authors contributed equally to this work.

http://dx.doi.org/10.1016/j.virol.2014.12.006
0042-6822/

the non-structural 1 (NS1) protein because of its short length, high copy number in infected cells, and redundant functions in antagonizing innate immunity (Hale et al., 2008; Palese, 2007). The NS1 protein is encoded on a collinear mRNA derived from the smallest vRNA segment eight, which is alternatively spliced to produce the nuclear export protein (NEP) mRNA, and is expressed to 10% the levels of NS1 (Lamb and Lai, 1980; Paterson and Fodor, 2012). Virus assembly requires NEP, thus genetic modifications that yield differences in levels of expression can hinder successful virus rescue or attenuate the virus (Paterson and Fodor, 2012).

To evaluate viral infection *in vitro* and *ex* or *in vivo*, fluorescent viruses are advantageous because secondary steps such as immunofluorescence staining or addition of bioluminescence substrates are not required to detect infected cells (Kayali et al., 2008; Kumar and Henrickson, 2012). A green fluorescent protein (GFP)-expressing IAV has been described (Kittel et al., 2004; Manicassamy et al., 2010), but its use is limited due to spectral overlap of GFP and tissue autofluorescence (Vintersten et al., 2004) or when GFP-expressing animals or cell lines serve as hosts of infection (Miller, 2011). As an alternative reporter, red fluorescent proteins have an excitation and emission spectra that is more conducive to *in vivo* or *ex vivo* imaging, offering less autofluorescence and deeper tissue penetrance (Shaner et al., 2005, 2007). Furthermore, laboratory evolution of red fluorescent proteins has led to a molecule, mCherry, that possesses higher quantum yield, a longer half-life, and that does not aggregate, as opposed to its ancestral protein derived from *Discosoma sp.* (Shaner et al., 2005).

Here, we describe for the first time the generation of replication-competent red fluorescent IAVs, where the NS1 protein of A/Puerto Rico/08/1934 (H1N1; PR8) is fused to mCherry, and the remaining seven segments are derived from PR8 or A/California_NYICE_E3/04/2009 (pH1N1). *In vitro*, mCherry IAVs are neutralized by monoclonal antibodies or inhibited by antivirals similarly to wild-type (WT) recombinant viruses, representing an excellent option for the rapid identification of neutralizing antibodies or antivirals using high-throughput screening. In mice, PR8 mCherry replication can be directly visualized and quantified from whole excised lungs using an *in vivo* imaging system (IVIS). These results offer a promising option to directly study the biology of influenza virus and to evaluate experimental countermeasures to treat influenza viral infections *in vitro* and *ex vivo.*

Results

Generation of a recombinant influenza A PR8 virus expressing the mCherry fluorescent protein

Generation of replication-competent reporter-expressing IAV requires that the inserted reporter gene neither impair critical functions of the protein(s) encoded by the native gene segment to which it is appended nor disrupt the packaging signals therein. The NS1 protein has previously been shown to tolerate fusion to foreign proteins including GFP (Kittel et al., 2004; Manicassamy et al., 2010; Perez et al., 2013), and thus is an ideal viral protein for reporter gene conjugation. However, red fluorescent proteins are preferred for *in vivo* studies (Shaner et al., 2005, 2007). Because the NS segment is alternatively spliced to produce NEP, two silent mutations were introduced in the splice acceptor site to avoid splicing (Hale et al., 2008; Kochs et al., 2007). To produce NEP, the porcine teschovirus-1 (PTV-1) 2A autoproteolytic cleavage site was inserted between NS1 and NEP so that both proteins (NS1 and NEP) would be translated individually (Fig. 1), like previously described (Manicassamy et al., 2010). Importantly, the NS1 and NEP N-terminal overlapping open reading frame was duplicated downstream of the PTV-1 2A site to assure NEP synthesis (Paterson and Fodor, 2012). Using two unique BsmBI restriction sites, mCherry was cloned and fused to NS1 and used to generate a recombinant PR8 NS1-mCherry virus (hereafter referred to as PR8 mCherry) using plasmid-based reverse genetics (Martinez-Sobrido and Garcia-Sastre, 2010).

Characterization of PR8 mCherry virus

To evaluate if PR8 encoding NS1 fused to mCherry could be directly visualized *in vitro* and to evaluate the subcellular localization of NS1 during PR8 WT and mCherry infection, fluorescence (mCherry) and indirect immunofluorescence microscopy were used (Fig. 2A and B). As expected, only cells infected with PR8 mCherry were fluorescent upon examination with a red filter. In cells infected with PR8 mCherry, the nuclear localization of NP (Fig. 2A) was similar to that of PR8 WT. Importantly, NS1 was similarly distributed in PR8 WT and mCherry infected cells (Fig. 2B).

PR8 WT and mCherry virus identity was then confirmed by RT-PCR and Western blotting (Fig. 2C and D). Expected band sizes of approximately 890 and 1891 nucleotides were amplified and resolved, corresponding to the NS vRNA from PR8 WT or mCherry, respectively (Fig. 2C). Additionally, primers amplifying the NS1-mCherry fusion only amplified an accurately sized band (1433 nt) from PR8 mCherry infected cells. As expected, NP mRNA levels were detected similarly from both PR8 WT and mCherry infected cells. We next evaluated protein expression by Western blotting using antibodies specific for NS1, mCherry, or NP as a control of viral infection (Fig. 2D). The amount of NS1 was slightly decreased in cells infected with PR8 mCherry as compared with PR8 WT, although NS1-mCherry was easily detected using the mCherry PAb. Differences between NS1 and NS1-mCherry signal intensities observed with the 1A7 monoclonal antibody correlate with a lower level of NP in PR8 mCherry infection, but may additionally be due to lower affinity of 1A7 when NS1 is fused to mCherry (Fig. 2D).

Growth properties of PR8 mCherry

Virus fitness in cell culture was next assessed by examining the multicycle growth properties and plaque formation of PR8 mCherry, as compared to PR8 WT (Fig. 3). PR8 mCherry viral kinetics were similar, albeit the total virus yield was lower after 24 h, with respect to PR8 WT (Fig. 3A). When evaluating the plaque phenotype, only PR8 mCherry formed fluorescent plaques (Fig. 3B), but in agreement with virus kinetics, the plaque size was slightly reduced compared to PR8 WT by immunostaining with an anti-NP monoclonal antibody (Fig. 3C). Importantly, all plaques detected using the anti-NP monoclonal antibody expressed mCherry (white arrows), indicating that all infectious viruses express mCherry.

Ability of NS1-mCherry fusion protein to inhibit IFNβ promoter activation

NS1 is a multifunctional protein that uses multiple mechanisms to counteract the type I interferon (IFN) response during viral infection (Hale et al., 2008). In order to evaluate if NS1-mCherry retained the ability to antagonize IFNβ activation, MDCK cells expressing GFP and FFluc under the control of the IFNβ promoter (Hai et al., 2008) were infected with PR8 WT and mCherry viruses (Fig. 4). As an internal control, cells were similarly infected with PR8 ΔNS1 (Garcia-Sastre et al., 1998), which potently induces IFNβ promoter activation (Geiss et al., 2002). GFP expression in infected cells indicated that PR8 mCherry infection inhibited IFNβ promoter activation to levels comparable to PR8 WT and, as expected,

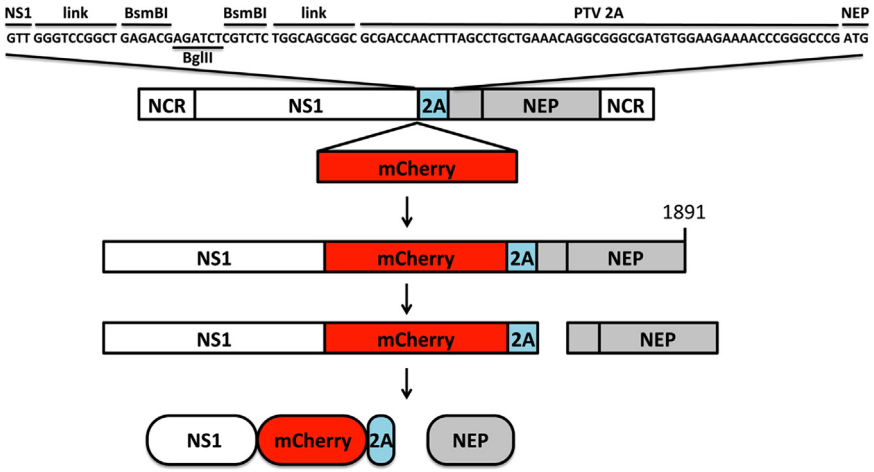

Fig. 1. Schematic representation of the modified IAV PR8 NS segments. IAV PR8 NS segment viral products are indicated by white (NS1) or gray (NEP) boxes. NCR denotes non-coding regions. Nucleotide length for the modified IAV PR8 NS segment is indicated. Sequences of mCherry and (PTV-1) 2A are indicated in red and blue boxes, respectively. (For interpretation of the references to color in this figure legend, the reader is referred to the web version of this article.)

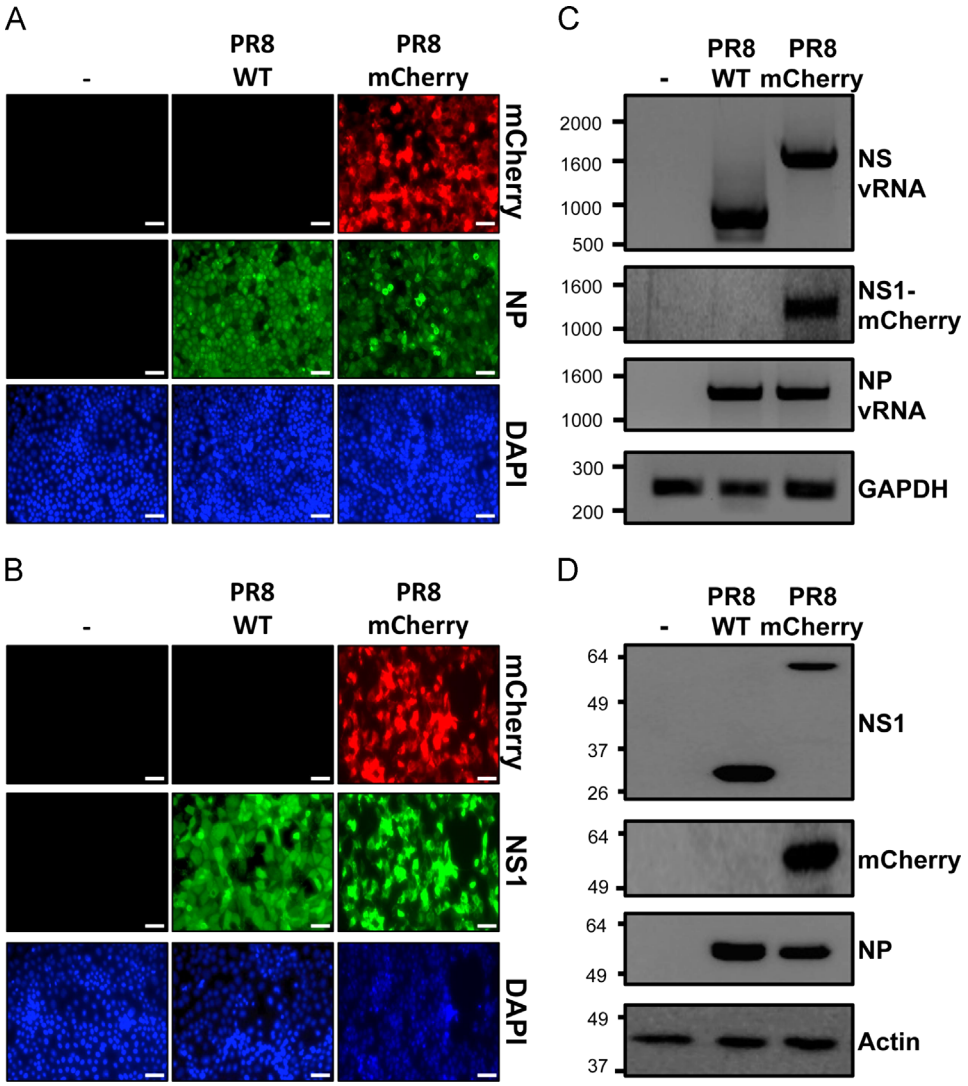

Fig. 2. Characterization of PR8 mCherry virus. MDCK cells were mock infected (-), or infected with PR8 WT or PR8 mCherry viruses. (A and B) Analysis of protein expression by fluorescence and immunofluorescence: At 18 h post-infection (MOI 0.1), cells were fixed, visualized for mCherry expression, and stained for PR8 NP (A) or NS1 (B). DAPI was used for nuclear staining. Representative images (20 × magnification) from three independent experiments are included. Scale bar, 100 μm. (C and D) Analysis of RNA and protein expression: At 18 h post-infection (MOI 1), RNA (C) and protein expression (D) were examined. cDNA synthesis for NS or NP vRNA was performed using IAV NS and NP vRNA specific primers. cDNA synthesis of mRNA was performed using oligo dT. Specific primers for PCR were used to amplify NS and NP vRNAs and mRNA for mCherry and cellular GAPDH as internal controls. Protein expression levels for NS1, NP and mCherry were evaluated using protein specific antibodies. Actin was used as a loading control. Numbers indicate the size of molecular markers in nucleotides (C) or kDa (D) for DNA and protein products, respectively.

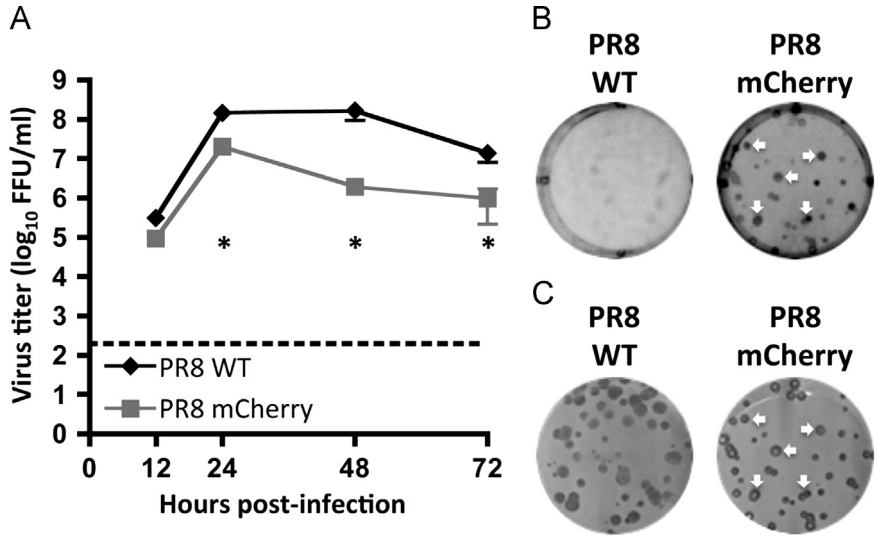

Fig. 3. Growth kinetics and plaque morphology of PR8 WT and mCherry viruses. (A) Multicycle growth kinetics. Virus titers from tissue culture supernatants of PR8 WT and mCherry infected (MOI 0.001) MDCK cells at the indicated times post-infection were analyzed by immunofocus assay (FFU/ml). Data represent the means ± SD of triplicates. Dotted line denotes the limit of detection (200 FFU/ml). $^*P < 0.05$ using an unpaired two-tailed Student's t test ($n=3$ per time point). (B and C) Plaque phenotype. Plaque sizes of PR8 WT and mCherry viruses in MDCK cells were evaluated 3 days post-infection by fluorescence (B) and immunostaining (C) using the HT103 NP monoclonal antibody. White arrows indicate correlation between mCherry fluorescent and NP positive plaques with the PR8 mCherry.

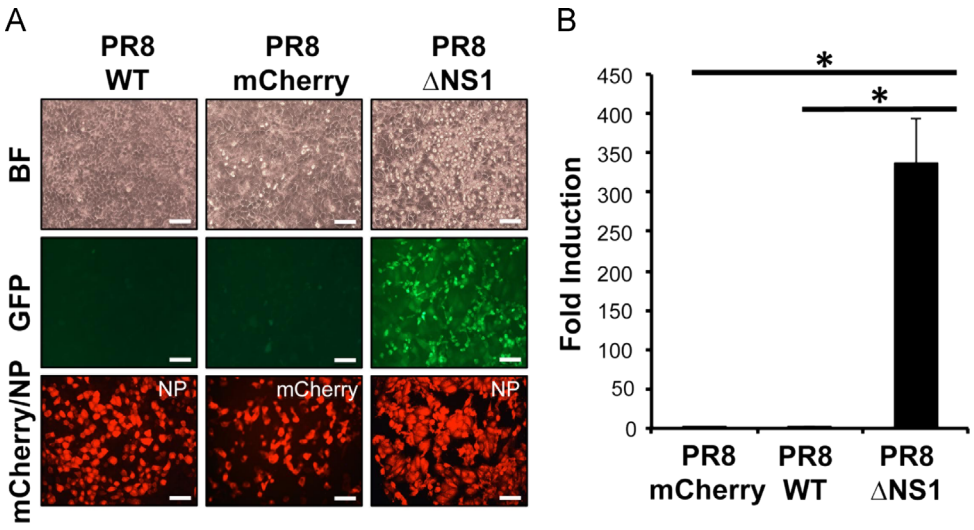

Fig. 4. Analysis of IFNβ promoter activation by PR8 mCherry virus: MDCK pIFNβ-GFP/IFNβ-FFluc cells were infected (MOI 2) with PR8 WT, mCherry, or ΔNS1 viruses and analyzed for IFNβ promoter activation 10 h post-infection. (A) IFNβ promoter activation by GFP expression: Activation of IFNβ promoter (GFP) and infection with PR8 mCherry was visualized directly with a fluorescence microscope. Infection of PR8 WT and ΔNS1 PR8 viruses was visualized by NP immunostaining using the HT103 MAb. Representative fields (20 × magnification) are shown. Scale bar, 100 μm. (B) IFNβ promoter activation by luciferase expression: Extracts from cells infected as in panel A were evaluated for IFNβ promoter activation by FFluc expression. Data show means ± SD of the results from triplicate samples. The induction of IFNβ was represented as fold induction relative to values from mock-infected cells. $^*P < 0.05$ using an unpaired two-tailed Student's t test ($n=3$ per time point).

PR8 ΔNS1 failed to inhibit IFNβ promoter activation (Fig. 4A). Similar results were obtained by analyzing luciferase expression from infected cell extracts (Fig. 4B).

Use of IAV expressing mCherry for the identification of antivirals and neutralizing antibodies

Identification of compounds that inhibit IAV generally require the use of secondary visualization approaches to evaluate viral infection (Beyleveld et al., 2013). An alternative approach for the identification of IAV antivirals, compatible with high-throughput screening, is urgently needed to identify new antivirals that overcome virus resistance. To demonstrate that IAV expressing mCherry is a valid surrogate to identify antivirals, we examined the ability of A3 (Hoffmann et al., 2011) and ribavirin (Cheung et al., 2014) to inhibit mCherry virus expression (Fig. 5A and B). A3 is a small molecule inhibitor of *de novo* pyrimidine biosynthesis that has been shown to inhibit IAV infection *in vitro* (Hoffmann et al., 2011), however, the compound has yet to be tested against the pH1N1 strain. Therefore, we first sought to rescue a recombinant pH1N1 virus containing the NS1-mCherry from PR8 (pH1N1 mCherry), using similar reverse genetics approaches to those described for rescuing PR8 mCherry, and to evaluate the inhibitory capacity of A3 against PR8 and pH1N1 mCherry viruses. Efficient virus rescue first indicated that the PR8 NS mCherry construct could be used in another H1N1 virus backbone. At high concentrations of ribavirin or A3 (starting concentration of 100 or 20 μM, respectively), PR8 mCherry was inhibited in a dose-dependent manner, as determined by mCherry expression via fluorescence microscopy (data not shown) or a plate reader (Fig. 5A). Similarly, pH1N1 mCherry was also inhibited (Fig. 5B), but the pandemic strain was less sensitive to A3 as compared to PR8 (Table 1).

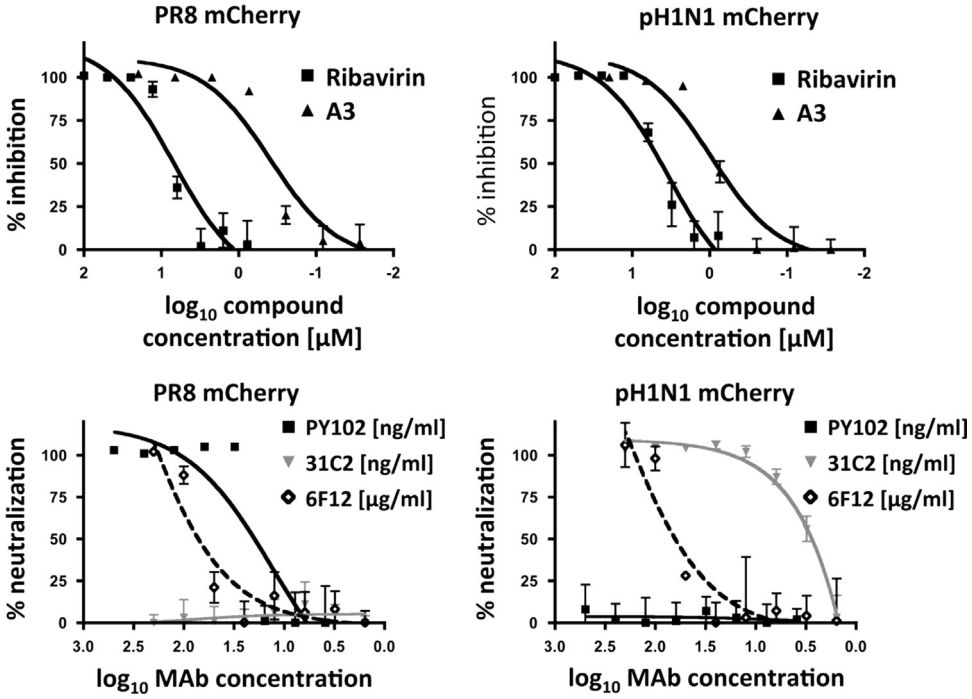

Fig. 5. A fluorescence-based assay for the identification of IAV antivirals (A and B) and neutralizing antibodies (C and D). Antivirals: MDCK cells were infected (MOI 0.005) with PR8 (A) or pH1N1 (B) mCherry viruses and incubated with serial dilutions of ribavirin (starting concentration 100 μM, 2-fold dilutions) or A3 (starting concentration 20 μM, 3-fold dilutions) for 24–36 h. As a control, infected cells were not treated. Sigmoidal dose response curves for PR8 (A) or pH1N1 (B) mCherry expression were evaluated using a fluorescence microplate reader. Percent inhibition was normalized to infection in the absence of drug. Data show means ± SD of the results determined for triplicates. Neutralizing antibodies: MDCK cells were infected (MOI 0.005, 24–36 h) with PR8 (C) or pH1N1 (D) mCherry viruses that were pre-incubated with 2-fold serial dilutions of HA specific monoclonal antibodies PY102 (PR8, starting concentration, 500 ng/ml), 31C2 (pH1N1, starting concentration, 200 ng/ml) and 6F12 (pan-H1, starting concentration, 200 μg/ml). Viruses in the absence of antibodies were used as internal control. Sigmoidal dose response curves for PR8 (C) or pH1N1 (D) mCherry expression were evaluated using a fluorescence microplate reader. Percent neutralization was normalized to infection in the absence of antibody. Note that monoclonal antibodies PY102 and 31C2 concentrations are in ng/ml $\log_{10}$ scale, while monoclonal antibody 6F12 concentration is in μg/ml $\log_{10}$ scale. Data show means ± SD of the results determined for triplicates.

Table 1
IC_{50} of compounds by fluorescence-based assay.

	IC50[a]	
Virus	Ribavirin	A3
PR8 mCherry	6.944	0.3956
pH1N1 mCherry	3.476	0.9556

[a] Compound concentration (μM) determined by serial-titration of drug with triplicate infections.

Table 2
IC_{50} of compounds by FFU titration method.

	IC50[a]	
Virus	Ribavirin	A3
PR8 WT	3.994	0.4828
PR8 mCherry	1.41	1.08
pH1N1 WT	13.98	8.735
pH1N1 mCherry	3.938	11.14

[a] Compound concentration (μM) determined by serial-titration of drug with triplicate infections.

To validate the sensitivity of the mCherry viruses to these antivirals, recombinant PR8 and pH1N1 WT and mCherry viruses were tested in antiviral assays that measure virus output (Bauman et al., 2013). Virus release into tissue culture supernatants were determined by immunofocus assay (fluorescent focus units, FFU), using an NP monoclonal antibody. All virus titers were determined across the same dilution series, and IC_{50} values calculated using a sigmoidal dose–response curve (Table 2). Regardless of the drug or IAV strain used, WT and mCherry IC_{50} values were similar, within 1–2 dilution values, and consistent with those in the literature (Hoffmann et al., 2011; Nguyen et al., 2009, 2010). Interestingly, both fluorescence and classic approaches indicate that pH1N1 is more resistant to A3 compared to PR8.

Similar to antiviral evaluation, virus neutralization assays to determine antibody-mediated virus inhibition require the use of secondary approaches to detect the presence of the virus, such as cell staining, immunofluorescence assay, ELISA or hemagglutination assays (Bauman et al., 2013; Webster and Stoehr, 2002). To overcome this additional step, PR8 and pH1N1 mCherry viruses were used to evaluate the neutralizing activity of monoclonal antibodies specific for PR8 (PY102) (Dinca et al., 1993), pH1N1 (31C2) (Medina et al., 2010) or both PR8 and pH1N1 (pan-H1 stalk-reactive monoclonal antibody 6F12) (Tan et al., 2012) by fluorescence expression using fluorescence microscopy (data not shown) or a fluorescence plate reader (Fig. 5C and D). PR8 mCherry was specifically neutralized by PY102 but not 31C2 monoclonal antibodies (Fig. 5C), whereas pH1N1 was neutralized by 31C2 but not PY102 (Fig. 5D). Both mCherry IAVs were neutralized by the pan-H1 6F12 monoclonal antibody. Additionally, we used a conventional virus neutralization assays to evaluate if, relative to WT IAVs, mCherry IAVs were comparably inhibited (Tables 3 and 4). The results show that specific neutralization was observed in a manner similar to the fluorescence approach and to previous reports (Baker et al., 2013; Dinca et al., 1993; Medina et al., 2010; Tan et al., 2012). These data demonstrate that mCherry IAVs can be used to evaluate both head- and stalk-reactive neutralizing antibodies using a fluorescence-based microneutralization assay. Altogether, these studies demonstrate that mCherry IAVs can be used to identify novel antivirals or neutralizing

Table 3
NT_{50} of MAbs by fluorescence-based assay.

	NT_{50}[a]		
Virus	PY102 (ng/ml)	31C2 (ng/ml)	6F12 (μg/ml)
PR8 mCherry	12.95	N/A	338.7
pH1N1 mCherry	N/A	3.152	231.5

[a] MAb concentration determined by serial-titration of Ab with triplicate infections. N/A, not applicable.

Table 4
NT_{50} of MAbs by VN assay.

	NT_{50}[a] (SD)		
Virus	PY102 (ng/ml)	31C2 (ng/ml)	6F12 (μg/ml)
PR8 WT	44 (22)	> 200 (0)	> 200 (0)
PR8 mCherry	44 (22)	> 200 (0)	> 200 (0)
pH1N1 WT	> 500 (0)	140 (71)	> 200 (0)
pH1N1 mCherry	> 500 (0)	100 (110)	> 200 (0)

[a] MAb concentration determined by serial-titration of Ab with triplicate infections.

antibodies without the use of secondary methodologies to determine viral infection and are therefore more compatible with high-throughput screening.

PR8 mCherry virus infection in mice

Next, we evaluated if PR8 mCherry was pathogenic in mice as a surrogate for virus replication. If PR8 mCherry replicates within inoculated mouse lungs, mCherry expression could potentially be used for virus detection and/or quantification. To that end, we first assessed the mouse lethal dose 50 (MLD_{50}) of PR8 mCherry by intranasally (i.n.) inoculating mice ($n=6$) with 10^2, 10^3, 10^4 or 10^5 FFU of PR8 mCherry and monitored body weight loss and mortality daily for two weeks (Fig. 6). All mice inoculated with 10^5 or 10^4 FFU succumbed to viral infection, whereas four out of 6 mice inoculated with 10^3 FFU survived. All mice inoculated with 10^2 FFU survived viral infection (Figs. 6A and B). Using the method of Reed and Muench (Reed, 1938), the MLD_{50} of PR8 mCherry is 1.8×10^3 FFU, which although not directly compared here, is ~50–100 times higher than PR8 WT (10–50 FFU, tested in age/sex/breed-matched mice) (Nogales et al., 2014). Thus PR8 mCherry can lead to a lethal infection in mice, likely caused by virus replication *in vivo*.

Kinetics of PR8 mCherry protein expression in mouse lungs

To evaluate mCherry fluorescence *ex vivo*, lungs from mice inoculated with 10^2, 10^3, 10^4 or 10^5 FFU of PR8 WT or mCherry were surgically removed three days post-infection, and fluorescence was quantified with an IVIS Spectrum multispectral imaging instrument (Fig. 7A). When mean radiant efficiency was determined for regions of interest corresponding to lung explants ($n=3$), a dose-dependent fluorescence intensity increase was detected in PR8 mCherry-infected mice that peaked with a dose of 10^4 FFU (Fig. 7B) at this time point. Viral infection was also quantified by determining viral titers (Fig. 7C). As expected, presence of PR8 mCherry in mice lungs was proportional to and greater than the amount of virus used for mice inoculations, and corroborated the MLD_{50} observations, that PR8 mCherry can replicate within lung tissue.

Lastly, the time-dependent kinetics of PR8 mCherry replication and fluorescence expression were evaluated in mouse lungs (Fig. 8). To that end, mice ($n=3$) were i.n. inoculated with

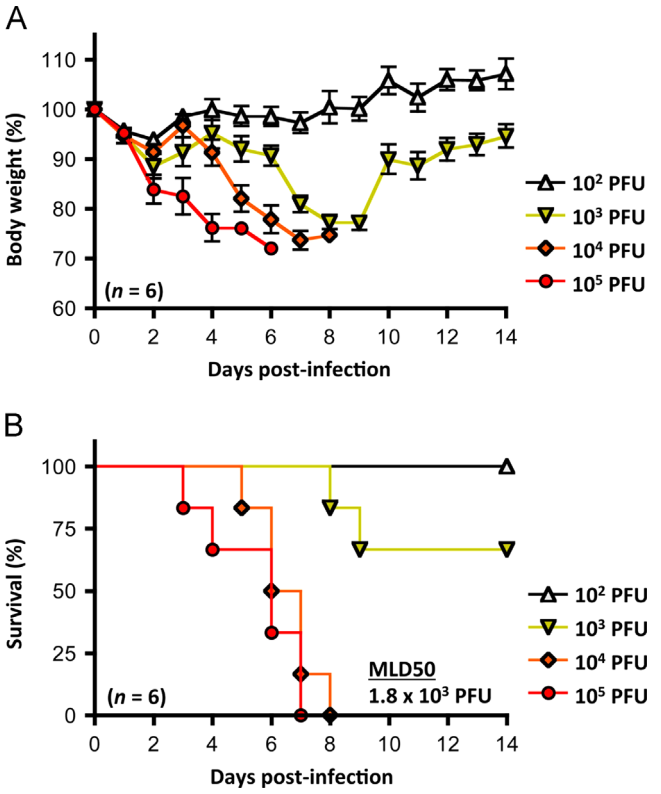

Fig. 6. Virulence of PR8 mCherry in mice: Female 6-to-8-week-old C57BL/6 mice ($n=6$) were i.n. inoculated with 10^2, 10^3, 10^4 or 10^5 FFU of PR8 mCherry and monitored daily for 2 weeks for body weight loss (A) and survival (B). Mice that lost 25% or greater of their initial body weight were sacrificed. The MLD_{50} for PR8 mCherry was determined by the method of Reed and Muench (Reed, 1938). Data represent means ± SEM of the results determined for individual mice.

10^5 FFU of PR8 mCherry and evaluated for fluorescence expression and viral titers at days 2, 4 and 6 post-infection. Due to the lack of fluorescence expression in PR8 WT inoculated mice (Fig. 7), PBS inoculated mice were further used as controls. In agreement with Fig. 7, mCherry expression was easily observed over background (PBS-inoculated naïve animals, Fig. 8A) at all days post-infection and peaked at day 4 post-infection. This was confirmed when mean radiant efficiency was calculated (Fig. 8B). Importantly, these results correlated with viral titers in lungs from infected animals (Fig. 8C). All together, these findings indicate that PR8 mCherry virus can be used to evaluate viral infection in mice lungs, and that in mice, the kinetics of PR8 mCherry virus infection are similar to that of recombinant PR8 WT virus infection (Nogales et al., 2014).

Discussion

Providing the ability to monitor viral infection in real time is advantageous to study the biology of IAV, to evaluate the effectiveness of current or potential antivirals, and to test the effectiveness of vaccine approaches. Here we describe the generation and characterization of replication-competent influenza A/Puerto Rico/8/34 (PR8) and A/California/04/09 (pH1N1) viruses expressing a red fluorescent mCherry protein as valid surrogates to facilitate the study of these viruses *in vitro* and *ex vivo*.

Both mCherry IAVs contain a recombinant PR8 NS segment that expresses the viral NS1 protein fused to mCherry. Co-linear NEP expression is maintained by shifting the entire NEP ORF downstream of the PTV-1 2A cleavage site (Fig. 1). IAV infection can be visualized in real time without the use of secondary antibodies or enzymes and vRNA and protein composition

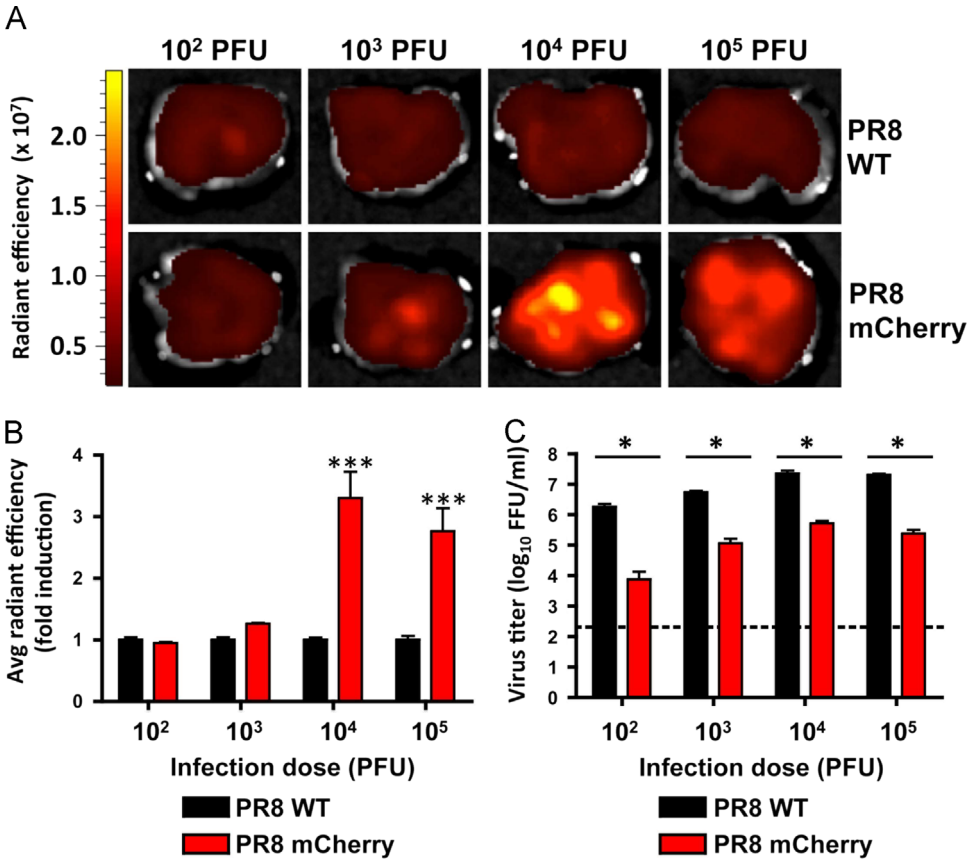

Fig. 7. Dose escalation and quantification of PR8 mCherry viral lung infection: Female 6-to-8-week-old C57BL/6 mice ($n=3$) were i.n. inoculated with 10^2, 10^3, 10^4 or 10^5 FFU of PR8 WT or mCherry viruses. Three days post-infection, lungs were harvested and fluorescence (A and B) and viral replication (C) were determined. A and B) Fluorescence imaging of whole lungs using IVIS: Representative fluorescence images with radiant efficiency heat maps overlaid (A) and mean values of regions of interest (B) were normalized to PR8 WT-infected mice at each dose, and induction of fluorescence determined. Columns represent mean ± SD. Statistical significance was calculated by using two-way ANOVA with Bonferonni post test; *** indicates P values < 0.001. (C) Viral lung titers: PR8 WT and mCherry replication in mice lungs were assessed by immunofocus assay (FFU/ml). Bars represent the mean ± SD of lung virus titers. Statistical analysis was conducted using the Student's t test. *$P < 0.05$ ($n=3$). Dotted line denotes the limit of detection (200 FFU/ml).

demonstrate insertion of mCherry (Fig. 2). As compared to PR8 WT, PR8 mCherry has similar, but slightly reduced replication kinetics and plaque size phenotype (Fig. 3), but maintains the ability to inhibit IFNβ promoter activation during viral infection (Fig. 4).

The only class of antivirals currently FDA-approved against circulating strains of IAV are neuraminidase (NA) inhibitors, and recent meta-analyses of clinical data suggests that treatment, although beneficial, does not decrease serious IAV complications (Jefferson et al., 2014). Thus, a rapid and sensitive assay to screen for anti-IAV compounds is urgently needed. Both PR8 and pH1N1 mCherry viruses were susceptible to dose-dependent inhibition by A3 and ribavirin (Fig. 5), yielding similar results as those obtained with PR8 and pH1N1 WT viruses (Tables 1 and 2). Moreover, the effectiveness of A3 against currently circulating pH1N1, pending its toxicity profile in humans, is a promising addition to the current anti-influenza treatment regime. The observation that pH1N1 was less susceptible to A3 than PR8 suggests differences in infected cell metabolism or polymerase substrate affinity. These results demonstrate the potential use of mCherry IAVs for high-throughput screening to identify novel antivirals without limitations associated with more laborious titration assays that are needed to quantitate WT virus.

Knowing that inhibition of IAV-driven mCherry expression correlated with a reduction in virus titer, we tested if mCherry IAV could be used to detect neutralizing antibodies via a fluorescence-based microneutralization assay and a fluorescence microplate reader (Fig. 5). Using well-characterized IAV monoclonal antibodies, our results demonstrate the feasibility to detect influenza strain-specific or broadly neutralizing antibodies using this approach. Importantly, similar neutralization titers were obtained with classic virus neutralization assays using recombinant PR8 and pH1N1 WT viruses (Tables 3 and 4). Without the need of secondary assays for viral quantification, large collections of hybridomas could potentially be evaluated, thereby simplifying their detection using high-throughput screening approaches.

Both ours and others' observations documented the attenuation of reporter-expressing IAV as compared to the recombinant WT virus (Fig. 6). For PR8 mCherry, high MLD_{50} values may be caused by altered levels of NS1 and/or NEP expression, which are known to affect viral replication both *in vitro* and *in vivo* (Bullido et al., 2001; Paterson and Fodor, 2012). Although the antagonism of innate immunity *in vivo* was not tested here, our *in vitro* results suggest that the anti-IFN function of NS1-mCherry is largely maintained. Importantly, both, the neutralizing activity of monoclonal antibodies or the antiviral activity of small molecule compounds could be evaluated in mice by directly evaluating mCherry expression from lungs of inoculated mice *ex vivo* since expression of mCherry in the excised whole lungs correlated with the amount of virus (Figs. 7 and 8).

Our strategy to express mCherry fused to IAV NS1 is similar to a NS1-GFP fusion recently described (Manicassamy et al., 2010). However, IAV NS1-mCherry seems to be more stable than IAV NS1-GFP since we have not observed NS1-mCherry viruses that lack expression of the fluorescent reporter. Nevertheless, the stability of NS1-mCherry and NS1-GFP viruses was not directly

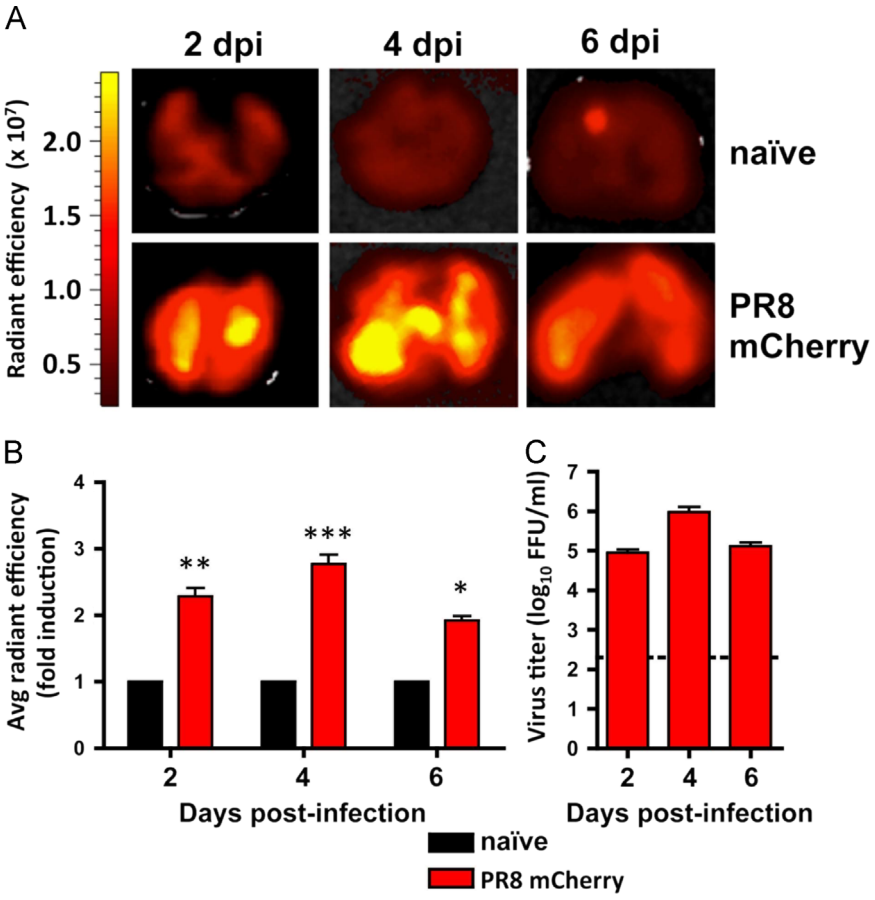

Fig. 8. Kinetics of PR8 mCherry infection in mouse lungs: Female 6-to-8-week-old C57BL/6 mice ($n=3$) were i.n. inoculated with PBS (naïve) or with 10^5 FFU of PR8 mCherry. At days 2, 4, and 6 post-infection (dpi), mice lungs were harvested for fluorescence (A and B) and production of infectious virus (C). (A and B) Fluorescence imaging of infected lungs: Lungs from mock-infected (naïve) and PR8 mCherry infected mice were harvested and analyzed by IVIS. (A) Representative fluorescence images with radiant efficiency heat maps overlaid. (B) Mean values of regions of interest were normalized to naïve mice at each time point, and induction of fluorescence was determined. Columns represent mean ± SD. Statistical significance was calculated using two-way ANOVA with Bonferonni post test; ***indicates P values < 0.001; **$P < 0.01$; *$P < 0.05$. (C) Viral lung titers: To evaluate virus replication, whole lungs were homogenized, and used to quantify viral titers by immunofocus assay (FFU/ml). Bars represent the mean ± SD of lung virus titers. Dotted line denotes the limit of detection (200 FFU/ml).

compared. Moreover, NS1-GFP virus cannot be used in *in vitro* and/or in *ex vivo* systems engineered to express GFP. Furthermore, red fluorescent proteins are better suited for *ex vivo* imaging due to natural green autofluorescence produced in tissue (Shaner et al., 2005, 2007).

Recombinant viruses expressing luciferase genes have also been reported (Heaton et al., 2013; Tran et al., 2013). Heaton et al. (2013) developed a replication-competent luciferase IAV by inserting the Gaussia luciferase (GLuc) reporter gene into the C-terminus of the PB2. PB2 and GLuc ORFs were separated with a 2A protease cleavage site, which cleaves the two proteins co-translationally. Similarly, Tran et al. (2013) engineered a replication-competent IAV reporter virus, suitable for *in vivo* imaging, that expressed NanoLuc luciferase separated with a 2A site of the viral PA gene. Although we have not yet detected IAV-driven mCherry expression in living mice, perhaps due to fluorescence intensity, an advantage of using fluorescent proteins instead of luciferases is that it is not necessary to inject luciferase substrates into the inoculated mice, as the amount of bioluminescent signal produced by luciferase depends on the efficiency of substrate delivery, which can be anatomically restrictive. Furthermore, because of the signal intensity and its retention within infected cells, mCherry is an ideal methodology to identify individually infected cells by intravital multiphoton imaging (Burrell et al., 2013; Gonzalez et al., 2010; Murooka and Mempel, 2013). Lastly, analysis of cells infected with fluorescent protein-expressing IAV is more rapid *in vitro*. With decreases in the analysis speed and cost, IAV mCherry opens the door for future studies to better understand the biology of influenza viruses as well as for high-throughput screening of both antivirals and neutralizing antibodies *in vitro* and *ex vivo*.

Materials and methods

Cell lines

MDCK and 293T cells were grown at 37 °C with 5% CO_2, in Dulbecco's modified Eagle's medium (DMEM) supplemented with 10% fetal bovine serum (FBS), and 1% PSG (penicillin, 100 units/ml; streptomycin 100 μg/ml; L-glutamine, 2 mM) (Nogales et al., 2014). MDCK cells expressing GFP and firefly luciferase (FFluc) genes under the control of the interferon (IFN) β promoter (MDCK pIFNβ-GFP/IFNβ-FFluc) were previously described (Hai et al., 2008).

Generation of the NS rescue plasmid containing NS1-mCherry fusion

To engineer a PR8 NS segment where the C-terminal of NS1 is fused to a gene of interest, we employed overlapping PCR and standard molecular biology techniques to introduce two BsmBI sites into an ambisense pDZ rescue plasmid (Schickli et al., 2001). This new plasmid, named pDZ-NS-2xBsmBI, contains the NS1 open reading frame (ORF), without the stop codon or splice acceptor site,

and two BsmBI sites followed by the porcine teschovirus-1 (PTV-1) 2A autoproteolytic cleavage site (ATNFSLLKQAGDVEENPGP) and NEP. The mCherry gene was then subcloned from a pCAGGS mCherry plasmid using oligonucleotides designed to introduce complementary BsmBI sites to generate the pDZ-NS-mCherry plasmid for viral rescues. Plasmid constructs were confirmed by sequencing (ACGT, Inc.). PR8 pDZ-NS-mCherry plasmid was used for the generation of PR8 and pH1N1 mCherry-expressing viruses.

Rescue of recombinant mCherry IAVs and viral kinetics

Recombinant WT and mCherry IAVs with the genetic backbone of PR8 (Baker et al., 2014; Nogales et al., 2014; Schickli et al., 2001) or pH1N1 (Baker et al., 2013; Medina et al., 2010) were rescued using previously described ambisense reverse genetics approaches (Fodor et al., 1999; Hoffmann et al., 2000; Martinez-Sobrido and Garcia-Sastre, 2010; Schickli et al., 2001). The viruses were plaque purified and amplified on MDCK cells to generate the viral stock used in this work. Multicycle virus growth kinetics were performed in MDCK cells (12-well plate format, 5×10^5 cells, triplicates) infected at low multiplicity of infection (MOI) of 0.001 as previously described (Baker et al., 2014; Bauman et al., 2013; Nogales et al., 2014). Mean value and standard deviation (SD) were calculated using Microsoft Excel software.

Protein gel electrophoresis and Western blot analysis

Cell extracts from either mock or virus-infected (MOI 1) MDCK cells (6-well plate format, 10^6 cells/well) at 18 h post-infection were lysed in passive lysis buffer (Promega) and analyzed for protein expression as previously described (Nogales et al., 2014) with the indicated primary monoclonal (MAb) or polyclonal (PAb) antibodies against mCherry (rabbit PAb Raybiotech), NS1 (mouse MAb 1A7) (Steidle et al., 2010), NP (mouse MAb HT103) (O'Neill et al., 1998) or actin (mouse MAb Sigma). Bound primary antibodies were detected with anti-mouse or anti-rabbit horseradish peroxidase (HRP)-conjugated secondary antibodies (1:2000 dilution, GE Healthcare). Protein bands were detected by chemiluminescence (Hyglo; Dennville Scientific Inc.).

RT-PCR

Mock and virus-infected (MOI 1) MDCK cells (6-well plate format, 10^6 cells/well) were harvested at 18 h post-infection and total RNA was purified using Trizol reagent (Invitrogen). cDNAs were synthesized using SuperScript® II Reverse Transcriptase (Invitrogen), using 0.5 μg of total RNA as template and an oligo-dT primer (to amplify total mRNAs) or specific primers for the NS and NP vRNAs. The cDNAs were used as templates for semi-quantitative PCR with primers specific for the NS and the NP vRNAs and for the NS1-mCherry and canine GAPDH mRNAs. Primers available upon request.

Plaque assays and viral titrations

Confluent MDCK cell monolayers (6-well plate format, 10^6 cells/well) were infected with 10-fold serial dilutions of PR8 WT or PR8 mCherry viruses. After infection, monolayers were overlaid with agar and incubated for 3 days at 37 °C. Cells were fixed with 4% paraformaldehyde (PFA), and the overlays were carefully removed. For visualization of mCherry, PBS was added and plates were imaged with a Kodak image station (4000 MM Pro molecular imaging system; Carestream Health, Inc., NY) (Rodrigo et al., 2011) and Kodak molecular imaging software (v5.0.1.30). Fixed cells were then permeabilized (0.5% Triton X-100 in PBS for 15 min at room temperature) and prepared for immunostaining as previously described (Baker et al., 2014) using the anti-NP MAb (HT103) and vector kits (Vectastain ABC kit and DAB HRP Substrate Kit: Vector), according to manufacturer's specifications. Where indicated, viral titers for both WT and mCherry viruses were determined by using specific MAbs for NP (HT103) (O'Neill et al., 1998) as previously described (FFU/ml) (Nogales et al., 2014).

Fluorescence and indirect immunofluorescence assays

MDCK cells were seeded on coverslips and mock-infected or infected (MOI 0.1) with PR8 WT or PR8 mCherry viruses. At 18 h post-infection, cells were fixed, permeabilized, and blocked with PBS/2.5% BSA. After blocking, specific MAbs for NP (HT103) (O'Neill et al., 1998) or NS1 (1A7) (Steidle et al., 2010) were diluted in blocking solution (1 μg/ml) and used to separately detect protein expression using a FITC-conjugated rabbit anti-mouse polyclonal secondary antibody (Dako, 1:200). Coverslips were mounted on glass slides with Prolong Gold (Invitrogen) containing 4′,6′-diamidino-2-phenylindole (DAPI, Research Organics). Images were captured using a fluorescence microscope (Nikon Eclipse TE2000), and processed using Adobe Photoshop CS4 (v11.0) software.

Cell-based type I interferon (IFN) assay

To evaluate the levels of IFN produced by infected cells, confluent monolayers of MDCK pIFNβ-GFP/IFNβ-FFluc cells (12-well plate format, 5×10^5 cells, triplicates) (Hai et al., 2008, Quinlivan et al., 2005) were infected (MOI 2) for 10 h with PR8 WT, PR8 ΔNS1 (Garcia-Sastre et al., 1998), or PR8 mCherry viruses. Infection levels were evaluated by mCherry or NP expression using fluorescence or immunofluorescence (NP MAb, HT103) as described above. Mean values and SDs were calculated using Microsoft Excel software. IFNβ promoter activation was represented as fold change relative to mock-infected cells.

Virus neutralization and fluorescence-based microneutralization assays

Virus neutralization assays were performed with PR8 and pH1N1 WT and mCherry viruses as previously described (Baker et al., 2014; Steel et al., 2009; Guo et al., 2011). Fluorescence-based microneutralization assays were performed with PR8 and pH1N1 mCherry viruses using a fluorescence plate reader (DTX-880, Becton Dickenson) (Martinez-Sobrido et al., 2010). Fluorescence values of mCherry virus infected cells in the absence of antibody were used to calculate 100% viral infection. Percent neutralization was calculated using the following equation: ([fluorescence value of indicated sera dilution − 100% infection]/100% infection) (1 0 0) (Rodrigo et al., 2011). Triplicate wells were used to calculate the mean and SD of neutralization, and inhibitory concentration 50 (IC_{50}) was determined by a sigmoidal dose response curve (Graphpad Prism, v4.0).

Antiviral assays

Antiviral-mediated inhibition of PR8 and pH1N1 WT and mCherry viruses was evaluated as previously described (Bauman et al., 2013) using 2- and 3-fold serial dilutions of ribavirin (Sidwell et al., 1972) or A3 (Hoffmann et al., 2011; Ortiz-Riano et al., 2014) at a starting concentration of 100 μM and 20 μM, respectively. Sigmoidal dose-response curves were generated (Graphpad Prism) to calculate IC_{50} values.

Mouse studies

Female 6-to-8-week-old C57BL/6 mice were purchased from the National Cancer Institute (NCI) and maintained in the animal care facility at the University of Rochester under specific pathogen-free conditions. Viral infections were performed as previously described (Nogales et al., 2014). Morbidity was monitored daily by body weight loss relative to starting weight. Mice showing more than 25% body weight loss were euthanized humanely. To evaluate viral replication, three mice per group were sacrificed at days 3 and 6 post-infection and lungs were removed and homogenized to calculate virus titers using an immunofocus assay (FFU/ml) as indicated above. Geometric mean titer (GMT) and statistical analysis (Mann–Whitney test) were performed using GraphPad Prism software (Nogales et al., 2014). The mouse lethal dose 50 (MLD_{50}) was determined by inoculating four groups of mice ($n=6$) with 10-fold serial dilutions of virus (10^5, 10^4, 10^3, and 10^2 FFU) and calculated using the method of Reed and Muench (Reed, 1938). Expression of mCherry in whole excised lungs was analyzed using an IVIS Spectrum multispectral imaging instrument (Caliper Life Sciences, Inc). Lungs were surgically extracted, washed with PBS, and images were acquired and analyzed with the Living Image 3.0 software to determine radiant efficiency of regions of interest [p/s/cm^2/sr] / [μW/cm^2]. Induction of fluorescence signal was normalized to WT- or mock-infected naïve animals. Statistical analysis (two-way ANOVA, bonferonni post-test) was performed using GraphPad Prism software (v4.0).

Acknowledgments

We thank Dr. Thomas M. Moran at the Center for Therapeutic Antibody Discovery at the Icahn School of Medicine at Mount Sinai for the HT103 monoclonal antibody. We also thank Drs. Peter Palese and Adolfo García-Sastre (Icahn School of Medicine at Mount Sinai) for the influenza PR8 and pH1N1 reverse genetics. S.F.B. is currently supported by the University of Rochester immunology training grant AI 007285-26. This research was funded by the 2014 University of Rochester Research Award to LM-S.

References

Ali, A., Avalos, R.T., Ponimaskin, E., Nayak, D.P., 2000. Influenza virus assembly: effect of influenza virus glycoproteins on the membrane association of M1 protein. J. Virol. 74, 8709–8719.

Avilov, S.V., Moisy, D., Munier, S., Schraidt, O., Naffakh, N., Cusack, S., 2012. Replication-competent influenza A virus that encodes a split-green fluorescent protein-tagged PB2 polymerase subunit allows live-cell imaging of the virus life cycle. J. Virol. 86, 1433–1448.

Baker, S.F., Guo, H., Albrecht, R.A., Garcia-Sastre, A., Topham, D.J., Martinez-Sobrido, L., 2013. Protection against lethal influenza with a viral mimic. J. Virol. 87, 8591–8605.

Baker, S.F., Nogales, A., Finch, C., Tuffy, K.M., Domm, W., Perez, D.R., Topham, D.J., Martinez-Sobrido, L., 2014. Influenza A and B virus intertypic reassortment through compatible viral packaging signals. J. Virol. 88, 10778–10791.

Bauman, J.D., Patel, D., Baker, S.F., Vijayan, R.S., Xiang, A., Parhi, A.K., Martinez-Sobrido, L., LaVoie, E.J., Das, K., Arnold, E., 2013. Crystallographic fragment screening and structure-based optimization yields a new class of influenza endonuclease inhibitors. ACS Chem. Biol. 8, 2501–2508.

Beyleveld, G., White, K.M., Ayllon, J., Shaw, M.L., 2013. New-generation screening assays for the detection of anti-influenza compounds targeting viral and host functions. Antiviral Res. 100, 120–132.

Bullido, R., Gomez-Puertas, P., Saiz, M.J., Portela, A., 2001. Influenza A virus NEP (NS2 protein) downregulates RNA synthesis of model template RNAs. J. Virol. 75, 4912–4917.

Burrell, K., Agnihotri, S., Leung, M., Dacosta, R., Hill, R., Zadeh, G., 2013. A novel high-resolution *in vivo* imaging technique to study the dynamic response of intracranial structures to tumor growth and therapeutics. J. Visualized Exp. JoVE, e50363.

Cheung, P.P., Watson, S.J., Choy, K.T., Fun Sia, S., Wong, D.D., Poon, L.L., Kellam, P., Guan, Y., Malik Peiris, J.S., Yen, H.L., 2014. Generation and characterization of influenza A viruses with altered polymerase fidelity. Nat. Commun. 5, 4794.

Dinca, L., Neuwirth, S., Schulman, J., Bona, C., 1993. Induction of antihemagglutinin antibodies by polyclonal antiidiotype antibodies. Viral Immunol. 6, 75–84.

Fodor, E., Devenish, L., Engelhardt, O.G., Palese, P., Brownlee, G.G., Garcia-Sastre, A., 1999. Rescue of influenza A virus from recombinant DNA. J. Virol. 73, 9679–9682.

Garcia-Sastre, A., Egorov, A., Matassov, D., Brandt, S., Levy, D.E., Durbin, J.E., Palese, P., Muster, T., 1998. Influenza A virus lacking the NS1 gene replicates in interferon-deficient systems. Virology 252, 324–330.

Geiss, G.K., Salvatore, M., Tumpey, T.M., Carter, V.S., Wang, X., Basler, C.F., Taubenberger, J.K., Bumgarner, R.E., Palese, P., Katze, M.G., Garcia-Sastre, A., 2002. Cellular transcriptional profiling in influenza A virus-infected lung epithelial cells: the role of the nonstructural NS1 protein in the evasion of the host innate defense and its potential contribution to pandemic influenza. Proc. Natl. Acad. Sci. U.S.A. 99, 10736–10741.

Gonzalez, S.F., Lukacs-Kornek, V., Kuligowski, M.P., Pitcher, L.A., Degn, S.E., Kim, Y.A., Cloninger, M.J., Martinez-Pomares, L., Gordon, S., Turley, S.J., Carroll, M.C., 2010. Capture of influenza by medullary dendritic cells via SIGN-R1 is essential for humoral immunity in draining lymph nodes. Nat. Immunol. 11, 427–434.

Guo, H., Santiago, F., Lambert, K., Takimoto, T., Topham, D.J., 2011. T cell-mediated protection against lethal 2009 pandemic H1N1 influenza virus infection in a mouse model. J. Virol. 85, 448–455.

Hai, R., Martinez-Sobrido, L., Fraser, K.A., Ayllon, J., Garcia-Sastre, A., Palese, P., 2008. Influenza B virus NS1-truncated mutants: live-attenuated vaccine approach. J. Virol. 82, 10580–10590.

Hale, B.G., Randall, R.E., Ortin, J., Jackson, D., 2008. The multifunctional NS1 protein of influenza A viruses. J. Gen. Virol. 89, 2359–2376.

Heaton, N.S., Leyva-Grado, V.H., Tan, G.S., Eggink, D., Hai, R., Palese, P., 2013. *In vivo* bioluminescent imaging of influenza a virus infection and characterization of novel cross-protective monoclonal antibodies. J. Virol. 87, 8272–8281.

Herfst, S., Schrauwen, E.J., Linster, M., Chutinimitkul, S., de Wit, E., Munster, V.J., Sorrell, E.M., Bestebroer, T.M., Burke, D.F., Smith, D.J., Rimmelzwaan, G.F., Osterhaus, A.D., Fouchier, R.A., 2012. Airborne transmission of influenza A/H5N1 virus between ferrets. Science 336, 1534–1541.

Hoffmann, E., Neumann, G., Hobom, G., Webster, R.G., Kawaoka, Y., 2000. "Ambisense" approach for the generation of influenza A virus: vRNA and mRNA synthesis from one template. Virology 267, 310–317.

Hoffmann, H.H., Kunz, A., Simon, V.A., Palese, P., Shaw, M.L., 2011. Broad-spectrum antiviral that interferes with de novo pyrimidine biosynthesis. Proc. Natl. Acad. Sci. U.S.A. 108, 5777–5782.

Jefferson, T., Jones, M.A., Doshi, P., Del Mar, C.B., Hama, R., Thompson, M., Spencer, E. A., Onakpoya, I., Mahtani, K.R., Nunan, D.N., Howick, J., Heneghan, C.J., 2014. Neuraminidase inhibitors for preventing and treating influenza in healthy adults and children. Sao Paulo Med. J.=Revista paulista de medicina 132, 256–257.

Kayali, G., Setterquist, S.F., Capuano, A.W., Myers, K.P., Gill, J.S., Gray, G.C., 2008. Testing human sera for antibodies against avian influenza viruses: horse RBC hemagglutination inhibition *vs.* microneutralization assays (The Official Publication of the Pan American Society for Clinical Virology). J. Clin. Virol. 43, 73–78.

Kilbourne, E.D., 2006. Influenza pandemics of the 20th century. Emerg. Infect. Dis. 12, 9–14.

Kittel, C., Sereinig, S., Ferko, B., Stasakova, J., Romanova, J., Wolkerstorfer, A., Katinger, H., Egorov, A., 2004. Rescue of influenza virus expressing GFP from the NS1 reading frame. Virology 324, 67–73.

Kochs, G., Garcia-Sastre, A., Martinez-Sobrido, L., 2007. Multiple anti-interferon actions of the influenza A virus NS1 protein. J. Virol. 81, 7011–7021.

Kumar, S., Henrickson, K.J., 2012. Update on influenza diagnostics: lessons from the novel H1N1 influenza A pandemic. Clin. Microbiol. Rev. 25, 344–361.

Lakdawala, S.S., Wu, Y., Wawrzusin, P., Kabat, J., Broadbent, A.J., Lamirande, E.W., Fodor, E., Altan-Bonnet, N., Shroff, H., Subbarao, K., 2014. Influenza a virus assembly intermediates fuse in the cytoplasm. PLoS Pathog. 10, e1003971.

Lamb, R.A., Lai, C.J., 1980. Sequence of interrupted and uninterrupted mRNAs and cloned DNA coding for the two overlapping nonstructural proteins of influenza virus. Cell 21, 475–485.

Li, F., Feng, L., Pan, W., Dong, Z., Li, C., Sun, C., Chen, L., 2010. Generation of replication-competent recombinant influenza A viruses carrying a reporter gene harbored in the neuraminidase segment. J. Virol. 84, 12075–12081.

Lopez-Martinez, I., Balish, A., Barrera-Badillo, G., Jones, J., Nunez-Garcia, T.E., Jang, Y., Aparicio-Antonio, R., Azziz-Baumgartner, E., Belser, J.A., Ramirez-Gonzalez, J.E., Pedersen, J.C., Ortiz-Alcantara, J., Gonzalez-Duran, E., Shu, B., Emery, S.L., Poh, M.K., Reyes-Teran, G., Vazquez-Perez, J.A., Avila-Rios, S., Uyeki, T., Lindstrom, S., Villanueva, J., Tokars, J., Ruiz-Matus, C., Gonzalez-Roldan, J.F., Schmitt, B., Klimov, A., Cox, N., Kuri-Morales, P., Davis, C.T., Diaz-Quinonez, J.A., 2013. Highly pathogenic avian influenza A(H7N3) virus in poultry workers, Mexico, 2012. Emerg. Infect. Dis. 19, 1531–1534.

Louie, J.K., Jean, C., Acosta, M., Samuel, M.C., Matyas, B.T., Schechter, R., 2011. A review of adult mortality due to 2009 pandemic (H1N1) influenza A in California. PLoS One 6, e18221.

Manicassamy, B., Manicassamy, S., Belicha-Villanueva, A., Pisanelli, G., Pulendran, B., Garcia-Sastre, A., 2010. Analysis of *in vivo* dynamics of influenza virus infection in mice using a GFP reporter virus. Proc. Natl. Acad. Sci. U.S.A. 107, 11531–11536.

Martinez-Sobrido, L., Cadagan, R., Steel, J., Basler, C.F., Palese, P., Moran, T.M., Garcia-Sastre, A., 2010. Hemagglutinin-pseudotyped green fluorescent protein-expressing influenza viruses for the detection of influenza virus neutralizing antibodies. J. Virol. 84, 2157–2163.

Martinez-Sobrido, L., Garcia-Sastre, A., 2010. Generation of recombinant influenza virus from plasmid DNA. J. Visualized Exp. JoVE.
Medina, R.A., Manicassamy, B., Stertz, S., Seibert, C.W., Hai, R., Belshe, R.B., Frey, S.E., Basler, C.F., Palese, P., Garcia-Sastre, A., 2010. Pandemic 2009 H1N1 vaccine protects against 1918 Spanish influenza virus. Nat. Commun. 1, 28.
Miller, R.L., 2011. Transgenic mice: beyond the knockout. Am. J. Physiol. Renal Physiol. 300, F291–300.
Molinari, N.A., Ortega-Sanchez, I.R., Messonnier, M.L., Thompson, W.W., Wortley, P.M., Weintraub, E., Bridges, C.B., 2007. The annual impact of seasonal influenza in the US: measuring disease burden and costs. Vaccine 25, 5086–5096.
Murooka, T.T., Mempel, T.R., 2013. Intravital microscopy in BLT-humanized mice to study cellular dynamics in HIV infection. J. Infect. Dis. 208 Suppl 2, S137–144.
Neumann, G., Watanabe, T., Ito, H., Watanabe, S., Goto, H., Gao, P., Hughes, M., Perez, D.R., Donis, R., Hoffmann, E., Hobom, G., Kawaoka, Y., 1999. Generation of influenza A viruses entirely from cloned cDNAs. Proc. Natl. Acad. Sci. U.S.A. 96, 9345–9350.
Nguyen, J.T., Hoopes, J.D., Le, M.H., Smee, D.F., Patick, A.K., Faix, D.J., Blair, P.J., de Jong, M.D., Prichard, M.N., Went, G.T., 2010. Triple combination of amantadine, ribavirin, and oseltamivir is highly active and synergistic against drug resistant influenza virus strains *in vitro*. PLoS One 5, e9332.
Nguyen, J.T., Hoopes, J.D., Smee, D.F., Prichard, M.N., Driebe, E.M., Engelthaler, D.M., Le, M.H., Keim, P.S., Spence, R.P., Went, G.T., 2009. Triple combination of oseltamivir, amantadine, and ribavirin displays synergistic activity against multiple influenza virus strains *in vitro*. Antimicrob. Agents Chemother. 53, 4115–4126.
Nogales, A., Baker, S.F., Ortiz-Riano, E., Dewhurst, S., Topham, D.J., Martinez-Sobrido, L., 2014. Influenza A virus attenuation by codon deoptimization of the NS gene for vaccine development. J. Virol. 88, 10525–10540.
O'Neill, R.E., Talon, J., Palese, P., 1998. The influenza virus NEP (NS2 protein) mediates the nuclear export of viral ribonucleoproteins. EMBO J. 17, 288–296.
Ortiz-Riano, E., Ngo, N., Devito, S., Eggink, D., Munger, J., Shaw, M.L., de la Torre, J.C., Martinez-Sobrido, L., 2014. Inhibition of arenavirus by A3, a pyrimidine biosynthesis inhibitor. J. Virol. 88, 878–889.
Ozawa, M., Kawaoka, Y., 2011. Taming influenza viruses. Virus Res. 162, 8–11.
Ozawa, M., Victor, S.T., Taft, A.S., Yamada, S., Li, C., Hatta, M., Das, S.C., Takashita, E., Kakugawa, S., Maher, E.A., Neumann, G., Kawaoka, Y., 2011. Replication-incompetent influenza A viruses that stably express a foreign gene. J. Gen. Virol. 92, 2879–2888.
Palese, P., 2007. Orthomyxoviridae: the viruses and their replication (ML). In: Knipe, D.M., Howley, P.M., Griffin, D.E., Lamb, R.A., Martin, M.A. (Eds.), Fields Virology, fifth ed. Lippincott Williams and WIlkins.
Pan, W., Dong, Z., Li, F., Meng, W., Feng, L., Niu, X., Li, C., Luo, Q., Li, Z., Sun, C., Chen, L., 2013. Visualizing influenza virus infection in living mice. Nat. Commun. 4, 2369.
Paterson, D., Fodor, E., 2012. Emerging roles for the influenza A virus nuclear export protein (NEP). PLoS Pathog. 8, e1003019.
Pena, L., Sutton, T., Chockalingam, A., Kumar, S., Angel, M., Shao, H., Chen, H., Li, W., Perez, D.R., 2013. Influenza viruses with rearranged genomes as live-attenuated vaccines. J. Virol. 87, 5118–5127.
Perez, J.T., Garcia-Sastre, A., Manicassamy, B., 2013. Insertion of a GFP Reporter Gene in Influenza Virus. Current Protocols in Microbiology Chapter 15, Unit 15G 14.
Quinlivan, M., Zamarin, D., Garcia-Sastre, A., Cullinane, A., Chambers, T., Palese, P., 2005. Attenuation of equine influenza viruses through truncations of the NS1 protein. J. Virol. 79, 8431–8439.
Reed, L.J., Muench, H., 1938. A simple method of estimating fifty percent endpoints. Am. J. Hyg. 27, 493–497.
Rimmelzwaan, G.F., Nieuwkoop, N.J., de Mutsert, G., Boon, A.C., Kuiken, T., Fouchier, R.A., Osterhaus, A.D., 2007. Attachment of infectious influenza A viruses of various subtypes to live mammalian and avian cells as measured by flow cytometry. Virus Res. 129, 175–181.
Rodrigo, W.W., de la Torre, J.C., Martinez-Sobrido, L., 2011. Use of single-cycle infectious lymphocytic choriomeningitis virus to study hemorrhagic fever arenaviruses. J. Virol. 85, 1684–1695.
Schickli, J.H., Flandorfer, A., Nakaya, T., Martinez-Sobrido, L., Garcia-Sastre, A., Palese, P., 2001. Plasmid-only rescue of influenza A virus vaccine candidates. Philos. Trans. R. Soc. London, Ser. B 356, 1965–1973.
Shaner, N.C., Patterson, G.H., Davidson, M.W., 2007. Advances in fluorescent protein technology. J. Cell Sci. 120, 4247–4260.
Shaner, N.C., Steinbach, P.A., Tsien, R.Y., 2005. A guide to choosing fluorescent proteins. Nat. Methods 2, 905–909.
Sidwell, R.W., Huffman, J.H., Khare, G.P., Allen, L.B., Witkowski, J.T., Robins, R.K., 1972. Broad-spectrum antiviral activity of Virazole: 1-beta-D-ribofuranosyl-1,2,4-triazole-3-carboxamide. Science 177, 705–706.
Smith, G.J., Vijaykrishna, D., Bahl, J., Lycett, S.J., Worobey, M., Pybus, O.G., Ma, S.K., Cheung, C.L., Raghwani, J., Bhatt, S., Peiris, J.S., Guan, Y., Rambaut, A., 2009. Origins and evolutionary genomics of the 2009 swine-origin H1N1 influenza A epidemic. Nature 459, 1122–1125.
Steel, J., Lowen, A.C., Pena, L., Angel, M., Solorzano, A., Albrecht, R., Perez, D.R., Garcia-Sastre, A., Palese, P., 2009. Live attenuated influenza viruses containing NS1 truncations as vaccine candidates against H5N1 highly pathogenic avian influenza. J. Virol. 83, 1742–1753.
Steidle, S., Martinez-Sobrido, L., Mordstein, M., Lienenklaus, S., Garcia-Sastre, A., Staheli, P., Kochs, G., 2010. Glycine 184 in nonstructural protein NS1 determines the virulence of influenza A virus strain PR8 without affecting the host interferon response. J. Virol. 84, 12761–12770.
Tan, G.S., Krammer, F., Eggink, D., Kongchanagul, A., Moran, T.M., Palese, P., 2012. A pan-H1 anti-hemagglutinin monoclonal antibody with potent broad-spectrum efficacy *in vivo*. J. Virol. 86, 6179–6188.
Tran, V., Moser, L.A., Poole, D.S., Mehle, A., 2013. Highly sensitive real-time *in vivo* imaging of an influenza reporter virus reveals dynamics of replication and spread. J. Virol. 87, 13321–13329.
Uyeki, T.M., Cox, N.J., 2013. Global concerns regarding novel influenza A (H7N9) virus infections. New Engl. J. Med. 368, 1862–1864.
Vintersten, K., Monetti, C., Gertsenstein, M., Zhang, P., Laszlo, L., Biechele, S., Nagy, A., 2004. Mouse in red: red fluorescent protein expression in mouse ES cells, embryos, and adult animals. Genesis 40, 241–246.
Webster R. G., C.N., Stoehr K., 2002. WHO Manual on Animal Influenza Diagnosis and Surveillance.
Wright, P.F., Neumann, G., Kawaoka, Y., 2007. Orthomyxoviruses. In: Knipe, D.M., Howley, P.M., Griffin, D.E., Lamb, R.A., Martin, M.A. (Eds.), Fields Virology, fifth ed. Lippincott Williams and WIlkins.